# *Modeling chemotaxis reveals the role of reversed phosphotransfer and a bi-functional kinase-phosphatase*

Article

Accepted Version

Rhodobacter chemotaxis 2010

# Modeling Chemotaxis Reveals the Role of Reversed Phosphotransfer and a Bi-Functional Kinase-Phosphatase

**Marcus J. Tindall[1,2,3*☯], Steven L. Porter[4,5*☯], Philip K. Maini[1,4], Judith P. Armitage[4]**

**1** Centre for Mathematical Biology, Mathematical Institute, University of Oxford, Oxford, United Kingdom, **2** Institute of Cardiovascular and Metabolic Research, School of Biological Sciences, University of Reading, Reading, United Kingdom, **3** Department of Mathematics, University of Reading, Reading, United Kingdom, **4** Oxford Centre for Integrative Systems Biology, Department of Biochemistry, University of Oxford, Oxford, United Kingdom, **5** School of Biosciences, University of Exeter, Exeter, United Kingdom

## Abstract

Understanding how multiple signals are integrated in living cells to produce a balanced response is a major challenge in biology. Two-component signal transduction pathways, such as bacterial chemotaxis, comprise histidine protein kinases (HPKs) and response regulators (RRs). These are used to sense and respond to changes in the environment. *Rhodobacter sphaeroides* has a complex chemosensory network with two signaling clusters, each containing a HPK, CheA. Here we demonstrate, using a mathematical model, how the outputs of the two signaling clusters may be integrated. We use our mathematical model supported by experimental data to predict that: (1) the main RR controlling flagellar rotation, $CheY_6$, aided by its specific phosphatase, the bifunctional kinase $CheA_3$, acts as a phosphate sink for the other RRs; and (2) a phosphorelay pathway involving $CheB_2$ connects the cytoplasmic cluster kinase $CheA_3$ with the polar localised kinase $CheA_2$, and allows $CheA_3$-P to phosphorylate non-cognate chemotaxis RRs. These two mechanisms enable the bifunctional kinase/phosphatase activity of $CheA_3$ to integrate and tune the sensory output of each signaling cluster to produce a balanced response. The signal integration mechanisms identified here may be widely used by other bacteria, since like *R. sphaeroides*, over 50% of chemotactic bacteria have multiple *cheA* homologues and need to integrate signals from different sources.

**Citation:** Tindall MJ, Porter SL, Maini PK, Armitage JP (2010) Modeling Chemotaxis Reveals the Role of Reversed Phosphotransfer and a Bi-Functional Kinase-Phosphatase. PLoS Comput Biol 6(8): e1000896. doi:10.1371/journal.pcbi.1000896

**Editor:** Christopher V. Rao, University of Illinois at Urbana-Champaign, United States of America

**Received** March 14, 2010; **Accepted** July 20, 2010; **Published** August 19, 2010



**Funding:** MJT and SLP were supported by research grant BB/C513350/1 from the Biological and Biotechnology Sciences Research Council (BBSRC). SLP was also supported by the Oxford Centre for Integrative Systems Biology (OCISB). PKM was partially supported by a Royal Society-Wolfson Research Merit award. The funders had no role in study design, data collection and analysis, decision to publish, or preparation of the manuscript.

**Competing Interests:** The authors have declared that no competing interests exist.

* E-mail: m.tindall@reading.ac.uk (MJT); s.porter@exeter.ac.uk (SLP)

☯ These authors contributed equally to this work.

## Introduction

Two-component signaling pathways are the major mechanism by which bacterial cells sense and respond to changes in their environment. They regulate processes as diverse as virulence, gene expression, development and motility [1]. Bacteria can have over 100 different two-component pathways per cell, one form of which controls swimming behavior. This chemosensory pathway has been extensively studied as an example of a two-component signaling pathway as it provides a model of signaling, signal termination and receptor adaptation. Mathematical modeling has proved particularly useful in helping to understand the complexity of *Escherichia coli* chemotaxis [2–10].

Most chemotactic bacteria sense changes in their extracellular environment using transmembrane chemoreceptors [11]. These chemoreceptors signal via an intracellular signaling cascade to the flagellar motor. In the case of *E. coli*, the signaling cascade is well understood [12,13]. The chemoreceptors form a quaternary complex at the cell poles with the scaffold protein CheW and the histidine protein kinase, CheA [14–16]. The chemoreceptors detect changes in the periplasmic chemoeffector concentration and control the rate at which CheA autophosphorylates on a conserved histidine residue. In response to decreased attractant concentration, the chemoreceptors signal to increase the rate of CheA autophosphorylation [17–19]. Following autophosphorylation, the phosphoryl group is transferred from the histidine residue of CheA to an aspartate residue in one of the two response regulators (RRs), CheY or CheB [20–22]. CheY-P is released from the chemotaxis cluster and diffuses through the cell to the flagellar motor. CheY-P binds the FliM component of the flagellar motors, causing the direction of flagellar rotation to switch from counter-clockwise to clockwise resulting in tumbling of the bacterium [23,24]. CheA-P also phosphorylates the methylesterase CheB, which facilitates adaptation of the chemoreceptor cluster [25,26]. CheY-P and CheB-P both naturally autodephosphorylate [27], although the rate of CheY-P dephosphorylation is enhanced by CheZ to allow signal termination within the time required for effective gradient sensing [28,29].

In contrast to *E. coli*, *Rhodobacter sphaeroides* has a more complex signaling pathway with multiple copies of the signaling proteins encoded by three major chemosensory operons [30]. Many other bacterial species appear to have multiple chemosensory operons as analysis of sequenced genomes suggests that ~50% of species with any *che* genes have at least two *cheA*s [30–32]. This raises the question of how behavior is controlled by two or more homologous pathways and how sensory data from each of the

## Author Summary

Chemotactic bacteria sense nutrient gradients and swim towards better environments for growth. A cluster of receptors in the cell membrane detects nutrient levels and signals via a cytoplasmic signaling pathway to the flagellum. The complexity of this signaling pathway varies across different bacterial species. The relatively simple pathway used by *Escherichia coli* is well understood; however, many bacteria, for example *Rhodobacter sphaeroides*, have more sophisticated pathways that, as well as being able to detect nutrients, are also able to assess the metabolic state of the cell. The receptors that detect metabolic state are located within an additional cluster that is physically distinct from the one that senses nutrients. In this work, we use a combination of experimentation and mathematical modeling to gain insight into the complex decision-making mechanisms that enable bacteria to weigh-up different stimuli and decide upon an appropriate response. We find novel communication mechanisms between the two signaling clusters that allow the outputs of the signaling pathways to be balanced and tuned according to the prevailing environmental conditions. The signaling principles identified here are likely to be used in other complex sensory networks.


pathways are integrated to produce a balanced response. Under laboratory conditions, *R. sphaeroides* swims using a single sub-polar unidirectional flagellum (Fla1), which is controlled by the protein products of *che*Op$_2$ and *che*Op$_3$ [33–38]. The intracellular signaling cascade controlling the Fla1 flagellum comprises three CheA kinase proteins (denoted CheA$_2$, CheA$_3$, CheA$_4$), three CheY proteins (CheY$_3$, CheY$_4$ and CheY$_6$) and two CheBs (CheB$_1$, CheB$_2$) [34,35,39–42]. CheA$_3$ and CheA$_4$ are unusual CheAs in that they lack some of the domains found in *E. coli* CheA and neither protein is capable of autophosphorylation [43]. However, together CheA$_3$ and CheA$_4$ have all of the activities of a functional CheA with CheA$_4$ forming a homodimer that binds ATP and phosphorylates the Hpt domain of CheA$_3$.

The signal transduction proteins are organized and localised into two distinct sensory clusters and the signaling output of both clusters is required for chemotaxis [43,44]. CheA$_2$ is located in a chemotaxis cluster at the cell poles, which comprises transmembrane chemoreceptors and the signal transduction proteins encoded by *che*Op$_2$ [44]. This cluster detects changes in the periplasmic concentration of chemoeffectors. Previous data show that CheA$_2$-P rapidly phosphorylates CheY$_3$, CheY$_4$, CheY$_6$, CheB$_1$ and CheB$_2$ (Figure 1), although the kinetics of phosphotransfer differ in each case [45]. CheA$_3$ and CheA$_4$ localize to a second chemotaxis cluster found in the cytoplasm [44]. This cluster contains the signal transduction proteins encoded by *che*Op$_3$ along with the soluble chemoreceptors and is believed to sense the metabolic state of the cell [44,46]. CheA$_3$-P rapidly phosphorylates only the RRs, CheY$_6$ and CheB$_2$ [43,47]. In addition, CheA$_3$ has an aspartyl-phosphate phosphatase activity that is specific for CheY$_6$-P; this activity is required for the rapid signal termination that is necessary for chemotactic responses [48]. CheA$_3$ in conjunction with CheA$_4$ can therefore be considered to be a bifunctional kinase/phosphatase.

*In vitro* studies have shown that all of the *R. sphaeroides* CheYs can bind the flagellar switch protein, FliM, and that this binding is strongest when the CheYs are phosphorylated [49], but less is known about the effect of CheY/CheY-P binding to FliM on flagellar rotation. CheY$_6$ is essential for chemotaxis and CheY$_6$-P alone is capable of causing the chemotactic stop that is necessary for changing swimming direction [39]. However, CheY$_6$ alone cannot support chemotaxis; either CheY$_3$ or CheY$_4$ are also required. Furthermore, phosphorylation site mutants of CheY$_3$, CheY$_4$ and CheY$_6$ do not support chemotaxis [39], suggesting that phosphorylation of all of these CheYs is necessary for chemotaxis.

Thus there are two complete chemosensory pathways in *R. sphaeroides*, localized to different regions of the cell and with different patterns and kinetics of phosphotransfer to the RRs. However, the outputs of these two signaling pathways must be

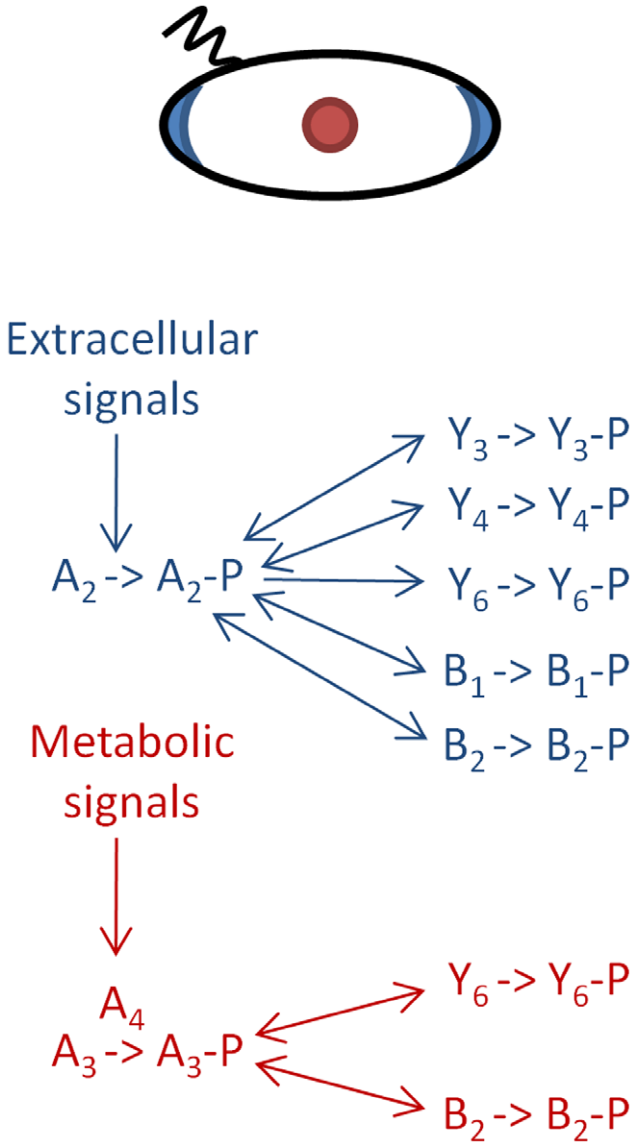


**Figure 1. Diagram showing the RRs phosphorylated by the polar (blue) and cytoplasmic (red) chemotaxis clusters.** The polar chemotaxis cluster contains CheA$_2$ and responds to the external environment. CheA$_2$ autophosphorylates and can then serve as a phosphodonor for all of the RRs. The cytoplasmic chemotaxis cluster contains CheA$_3$ and CheA$_4$, and is thought to respond to the metabolic state of the cell. CheA$_3$ is phosphorylated by CheA$_4$. Unlike CheA$_2$-P, CheA$_3$-P is not able to phosphorylate all of the RRs – it can only phosphorylate CheY$_6$ and CheB$_2$. All of the RR-Ps spontaneously autodephosphorylate; however, the dephosphorylation of CheY$_6$-P is accelerated by the phosphatase activity of CheA$_3$.
doi:10.1371/journal.pcbi.1000896.g001

integrated to control the behavior of a single flagellar motor. *In vitro* biochemistry identified which RRs are phosphorylated by each CheA and the kinetics of the interactions, however, assessing the relative contribution made to RR-P levels by each of these CheAs *in vivo* is more complex, since all of the RR-Ps will be competing with one another for phosphorylation by the CheAs. We used mathematical modeling to predict the possible signaling pathways within this complex system and tested these predictions experimentally.

The aim of this study was therefore to combine our knowledge of the kinetic preferences of the signaling reactions gained from *in vitro* biochemistry with the *in vivo* data on protein copy number within a mathematical model that can predict the changes in RR-P levels resulting from changes in CheA activity at either cluster. This model was then used to analyze the contribution made by each cluster in controlling RR-P levels and the dynamics of the signaling reactions. Using the model, we identified unexpected key roles for reversed phosphotransfer between RR-P and CheA in the network, which would enable communication between the two sensory clusters and thus regulate the output signals. In addition, we demonstrated that the principal RR, $CheY_6$, with the aid of its specific phosphatase, the bifunctional $CheA_3/CheA_4$ kinase, could act as a phosphate sink for the other RR-Ps. Regulation of the output of sensory networks by the activity of key kinase/phosphatase proteins is likely to be a common mechanism, but this is one of the first to be identified that balances the outputs of two interconnected pathways.

## Results

### Construction of the mathematical model

Within an *R. sphaeroides* cell, $CheA_2$ has been shown to localize to the polar chemotaxis cluster, while $CheA_3$ and $CheA_4$ localize to the cytoplasmic cluster [44]. All the *R. sphaeroides* CheYs are free to diffuse throughout the cytoplasm of the cell enabling communication between the receptor clusters and flagellar motor. Unlike *E. coli*, the CheBs are also diffuse in the cytoplasm [39,44]. As illustrated in Figure 1, $CheA_2$-P can phosphorylate all of the RRs, whilst $CheA_3$-P is only able to phosphorylate $CheY_6$ and $CheB_2$. What is the reason for this discrimination and how does it contribute towards the chemotactic response of the cell? To understand the role of each signaling cluster we constructed an ordinary differential equation (ODE) model of an *R. sphaeroides* cell as detailed in Text S1. The model integrates *in vivo* protein expression levels with *in vitro* data on the kinetic preference of the CheAs for each of the RRs to predict RR-P levels throughout a simulated chemotactic response. The model includes the phosphorylation reactions shown in Table 1 and was parameterized with published reaction rate constants and protein expression levels (Table 2).

The parameters for the phosphotransfer reactions were obtained by parameter fitting the previously published *R. sphaeroides* chemotaxis phosphotransfer assay data [43,45,48], where CheA-$^{32}$P served as a phosphodonor to the RRs (Table 3). In the few cases where the assays were not very sensitive to the rate of reversed phosphotransfer from RR-P to CheA, reliable estimates of these rates were obtained using alternative phosphotransfer assays, in which RR-P was mixed with unphosphorylated $CheA_2$ or $CheA_3$ (examples shown in Figure 2). In these reactions, RR-P was generated using purified phosphorylated CheA P1 domains (either $CheA_2$P1-P or $CheA_3$P1-P) as the phosphodonor; control reactions lacking RR showed no phosphotransfer from $CheA_2$P1-P or $CheA_3$P1-P to either $CheA_2$ or $CheA_3$. These experiments showed that while $CheA_2$ is phosphorylated by $CheB_2$-P (Figure 2C) it is not phosphorylated by $CheY_6$-P (Figure 2B). The parameter values obtained from these phosphotransfer reactions were then used in constructing the model.

**Table 1.** The phosphorylation reactions included in the model of the *R. sphaeroides* chemotaxis signalling pathway.

| Reaction number | Reaction | Type |
|---|---|---|
| (1) | $A_2 \xrightarrow{k_1} A_{2P}$ | Autophosphorylation |
| (2) | $A_3 \xrightarrow{k_2} A_{3P}$ | Phosphorylation by $CheA_4$ |
| (3) | $A_{2P} + Y_3 \underset{k_{-3}}{\overset{k_3}{\leftrightarrow}} A_2 + Y_{3P}$ | Phosphotransfer |
| (4) | $A_{2P} + Y_4 \underset{k_{-4}}{\overset{k_4}{\leftrightarrow}} A_2 + Y_{4P}$ | Phosphotransfer |
| (5) | $A_{2P} + Y_6 \underset{k_{-5}}{\overset{k_5}{\leftrightarrow}} A_2 + Y_{6P}$ | Phosphotransfer |
| (6) | $A_{2P} + B_1 \underset{k_{-6}}{\overset{k_6}{\leftrightarrow}} A_2 + B_{1P}$ | Phosphotransfer |
| (7) | $A_{2P} + B_2 \underset{k_{-7}}{\overset{k_7}{\leftrightarrow}} A_2 + B_{2P}$ | Phosphotransfer |
| (8) | $A_{3P} + Y_6 \underset{k_{-8}}{\overset{k_8}{\leftrightarrow}} A_3 + Y_{6P}$ | Phosphotransfer |
| (9) | $A_{3P} + B_2 \underset{k_{-9}}{\overset{k_9}{\leftrightarrow}} A_3 + B_{2P}$ | Phosphotransfer |
| (10) | $Y_{3P} \xrightarrow{k_{10}} Y_3$ | Autodephosphorylation |
| (11) | $Y_{4P} \xrightarrow{k_{11}} Y_4$ | Autodephosphorylation |
| (12) | $Y_{6P} \xrightarrow{k_{12}} Y_6$ | Autodephosphorylation |
| (13) | $B_{1P} \xrightarrow{k_{13}} B_1$ | Autodephosphorylation |
| (14) | $B_{2P} \xrightarrow{k_{14}} B_2$ | Autodephosphorylation |
| (15a) | $A_{3P} + Y_{6P} \xrightarrow{k_{15a}} A_{3P} + Y_6$ | Phosphatase assisted dephosphorylation |
| (15b) | $A_3 + Y_{6P} \xrightarrow{k_{15b}} A_3 + Y_6$ | Phosphatase assisted dephosphorylation |

doi:10.1371/journal.pcbi.1000896.t001

### Response regulator dephosphorylation rates show $CheY_6$ acts as a phosphate sink

*R. sphaeroides* responds to brief stimuli, returning to prestimulus behavior in less than 1 s [50]. This requires a rapid rate of signal termination. The measured autodephosphorylation half-times of the chemotaxis RRs, however, vary from ~4 s for $CheY_6$-P to ~4000 s for $CheB_1$-P (Table 4). As *R. sphaeroides* does not have a CheZ homologue, an alternative dephosphorylation mechanism is required. Recently, $CheA_3$ was shown to be a specific phosphatase for $CheY_6$-P [48], but no phosphatases have been identified for the remaining chemotaxis RRs.

Phosphate sinks have been shown to be involved in signal termination in several bacterial signaling pathways [51–54]. To test whether a similar mechanism operates in *R. sphaeroides*, we used the model to predict the decay timecourse of RR-P levels resulting from simultaneously switching off autophosphorylation of $CheA_2$ (reaction 1 in Table 1) and the phosphorylation of $CheA_3$ by $CheA_4$ (reaction 2 in Table 1). Although, the model incorporates the experimentally determined autodephosphorylation rates (reactions 10–15b of Table 1), interestingly, the model predicts that levels of all of the RR-Ps decay with half-lives shorter than ~7 s (Table 4), which is much faster than their experimen-

**Table 2.** Parameter values directly determined from experimental data.

| Rate | Description | Value | Standard error | Units | Source |
|---|---|---|---|---|---|
| $k_1$ | $CheA_2$ autophosphorylation | 0.12 | 0.02 | $s^{-1}$ | [45] |
| $k_2$ | Phosphorylation of $CheA_3$ by $CheA_4$ | 0.98 | 0.17 | $s^{-1}$ | [43] |
| $k_{10}$ | $CheY_{3P}$ autodephosphorylation | $1.93\times10^{-2}$ | $0.20\times10^{-2}$ | $s^{-1}$ | [45] |
| $k_{11}$ | $CheY_{4P}$ autodephosphorylation | $1.82\times10^{-2}$ | $0.13\times10^{-2}$ | $s^{-1}$ | [45] |
| $k_{12}$ | $CheY_{6P}$ autodephosphorylation | $1.69\times10^{-1}$ | $0.12\times10^{-1}$ | $s^{-1}$ | [45] |
| $k_{13}$ | $CheB_{1P}$ autodephosphorylation | $1.73\times10^{-4}$ | $0.06\times10^{-4}$ | $s^{-1}$ | [45] |
| $k_{14}$ | $CheB_{2P}$ autodephosphorylation | $1.33\times10^{-2}$ | $0.12\times10^{-2}$ | $s^{-1}$ | [45] |
| $k_{15a}$ | $CheY_{6P}$ dephosphorylation by $CheA_3$ | $5.20\times10^{3}$ | $0.32\times10^{3}$ | $(Ms)^{-1}$ | [48] |
| $k_{15b}$ | $CheY_{6P}$ dephosphorylation by $CheA_{3P}$ | $5.20\times10^{3}$ | $0.32\times10^{3}$ | $(Ms)^{-1}$ | [48] |
| $A_{2T}$ | Total concentration of $CheA_2$ | 89.9 | 7.6 | μM | [69] |
| $A_{3T}$ | Total concentration of $CheA_3$ | 89.9 | 10.4 | μM | [69] |
| $Y_{3T}$ | Total concentration of $CheY_3$ | 3.5 | 1.0 | μM | [68] |
| $Y_{4T}$ | Total concentration of $CheY_4$ | 13.8 | 2.8 | μM | [68] |
| $Y_{6T}$ | Total concentration of $CheY_6$ | 225 | 27 | μM | [68] |
| $B_{1T}$ | Total concentration of $CheB_1$ | 81.2 | 3.8 | μM | [69] |
| $B_{2T}$ | Total concentration of $CheB_2$ | 20.8 | 2.1 | μM | [69] |

doi:10.1371/journal.pcbi.1000896.t002

tally measured autodephosphorylation rates. Within the model, only $CheY_6$-P has a phosphatase. The only route by which the model could predict dephosphorylation rates for the other RR-Ps that are faster than their autodephosphorylation rates is for one or more of the RRs to be acting as ''phosphate sinks'', with the dephosphorylation of the target RR-P proceeding via reversed phosphotransfer to a CheA, which in turn transfers the phosphoryl group to the sink RR.

To determine which RRs could act as sinks, we simulated RR-P decay rates in cells deleted for a single RR e.g. for the cell lacking $CheY_3$ we changed $Y_{3T}$ to zero and measured the simulation half-lives of the remaining RR-Ps. We found that only the removal of $CheY_6$ greatly increased the simulation half-lives of the remaining RR-Ps (Table 4), suggesting that $CheY_6$ acts as a phosphate sink for all of the other RR-Ps. Without $CheY_6$, the simulation half-lives of the remaining RRs were in some cases ($CheY_3$-P, $CheY_4$-P and $CheB_2$-P) increased beyond their autodephosphorylation half-times (Table 4). This is the result of significant quantities of $CheA_3$-P and $CheA_2$-P being present at steady state, and persisting for some time after the autophosphorylation reactions (reactions 1 and 2) were turned off. This allows levels of RR-P to be replenished resulting in a RR-P simulation half-time that is slower than their autodephosphorylation half-times. Interestingly, even in the absence of $CheY_6$, the simulated dephosphorylation rate of $CheB_1$-P was faster than its autodephosphorylation rate. In the absence of $CheY_6$, the other RRs ($CheY_3$, $CheY_4$ and $CheB_2$) may act as phosphate sinks for $CheB_1$-P i.e. $CheB_1$-P acts as a phosphodonor for $CheA_2$ which in turn donates the phosphoryl

**Table 3.** Parameter values estimated indirectly by fitting to phosphotransfer reaction data.

| Rate | Description | Value | Units | Source |
|---|---|---|---|---|
| $k_3$ | $CheA_{2P}$ to $CheY_3$ phosphotransfer | $6.60\times10^{3}$ | $(Ms)^{-1}$ | This study using [45] |
| $k_{-3}$ | $CheA_{2P}$ to $CheY_3$ reverse phosphotransfer | $1.17\times10^{4}$ | $(Ms)^{-1}$ | This study using [45] |
| $k_4$ | $CheA_{2P}$ to $CheY_4$ phosphotransfer | $8.85\times10^{5}$ | $(Ms)^{-1}$ | This study using [45] |
| $k_{-4}$ | $CheA_{2P}$ to $CheY_4$ reverse phosphotransfer | $2.32\times10^{5}$ | $(Ms)^{-1}$ | This study using [45] |
| $k_5$ | $CheA_{2P}$ to $CheY_6$ phosphotransfer | $1.54\times10^{3}$ | $(Ms)^{-1}$ | This study using [45] |
| $k_{-5}$ | $CheA_{2P}$ to $CheY_6$ reverse phosphotransfer | 0 | $(Ms)^{-1}$ | This study |
| $k_6$ | $CheA_{2P}$ to $CheB_1$ phosphotransfer | $1.78\times10^{6}$ | $(Ms)^{-1}$ | This study using [45] |
| $k_{-6}$ | $CheA_{2P}$ to $CheB_1$ reverse phosphotransfer | $2.85\times10^{6}$ | $(Ms)^{-1}$ | This study using [45] |
| $k_7$ | $CheA_{2P}$ to $CheB_2$ phosphotransfer | $3.07\times10^{3}$ | $(Ms)^{-1}$ | This study using [45] |
| $k_{-7}$ | $CheA_{2P}$ to $CheB_2$ reverse phosphotransfer | $1.53\times10^{3}$ | $(Ms)^{-1}$ | This study |
| $k_8$ | $CheA_{3P}$ to $CheY_6$ phosphotransfer | $7.75\times10^{5}$ | $(Ms)^{-1}$ | This study using [43] |
| $k_{-8}$ | $CheA_{3P}$ to $CheY_6$ reverse phosphotransfer | $2.83\times10^{3}$ | $(Ms)^{-1}$ | This study using [43] |
| $k_9$ | $CheA_{3P}$ to $CheB_2$ phosphotransfer | $6.15\times10^{4}$ | $(Ms)^{-1}$ | This study using [43] |
| $k_{-9}$ | $CheA_{3P}$ to $CheB_2$ reverse phosphotransfer | $3.10\times10^{3}$ | $(Ms)^{-1}$ | This study using [43] |

doi:10.1371/journal.pcbi.1000896.t003

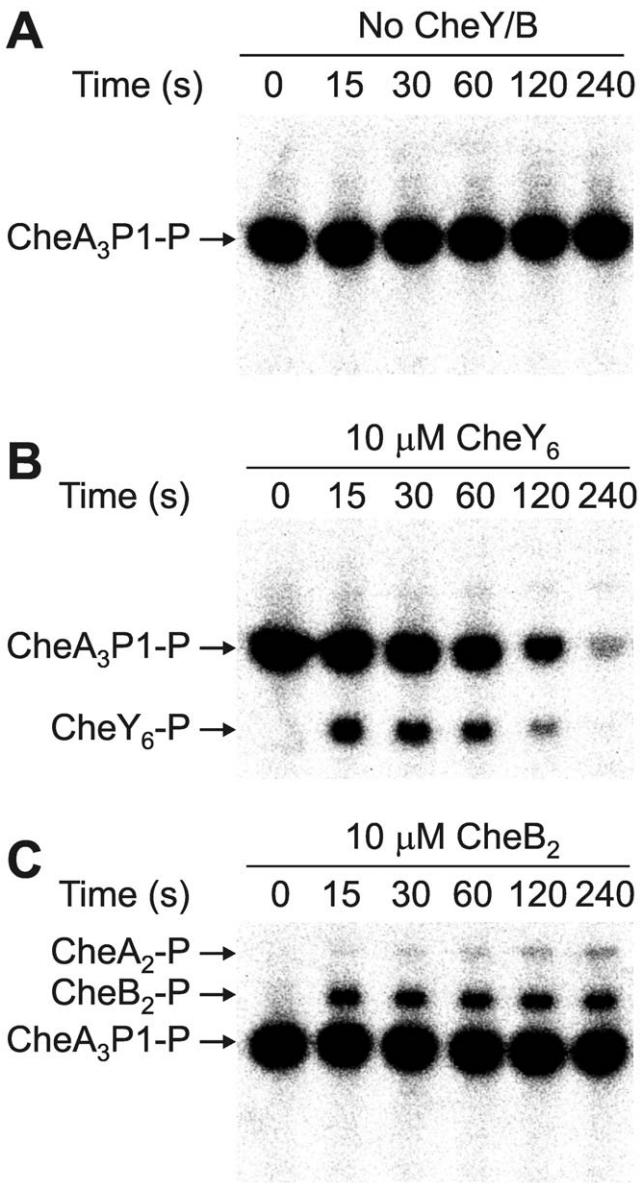


**Figure 2. Phosphorimages of SDS-PAGE gels measuring phosphotransfer rate from $CheY_6$-P and $CheB_2$-P to $CheA_2$.** 30 μM $CheA_3P1$-$^{32}P$ was incubated with 5 μM $CheA_2$ for 1 hour prior to the addition of (A) reaction buffer, (B) 10 μM $CheY_6$ and (C) 10 μM $CheB_2$. 10 μl reaction samples were then taken at the time points indicated and quenched in 20 μl of 1.5 X SDS/EDTA loading dye. The quenched samples were analyzed by SDS-PAGE and detected by phosphorimaging.
doi:10.1371/journal.pcbi.1000896.g002

groups to $CheY_3$, $CheY_4$ and $CheB_2$. To test this we set the rate of phosphotransfer from $CheB_1$-P to $CheA_2$ ($k_{-6}$) to zero and found that the simulated dephosphorylation half-time for $CheB_1$-P was increased to 4295 s, which is comparable with its autodephosphorylation half-time indicating that in the absence of $CheY_6$, one or more of other RRs therefore act as phosphate sinks for $CheB_1$.

To confirm that the ability of $CheY_6$ to act as a phosphate sink was robust to changes in parameters we performed a sensitivity analysis, where we varied each parameter by factors of 0.1, 0.5, 1.5 and 10, and measured the effect on the simulation half-life of $CheB_1$-P (Table S1). For the parameters that were determined experimentally, the standard error lies well within the range covered by factors of 0.5 and 1.5. The simulation half-life of $CheB_1$-P was robust to large changes in the majority of parameters, and in all cases remained much faster than the $CheB_1$-P autodephosphorylation rate, but as would be expected showed some sensitivity towards those parameters directly involved in the operation of the $CheY_6$ phosphate sink i.e. the rates of phosphotransfer between $CheB_1$ and $CheA_2$ and between $CheA_2$ and $CheY_6$. In addition, the system was also sensitive to large changes, well outside the range covered by experimental error in parameter determination, in the total concentrations of $CheA_2$ and $CheY_6$. This sensitivity analysis indicates that the parameter space in which the phosphate sink mechanism will work efficiently is broad and extends well beyond the range of experimental errors in the parameters themselves, suggesting that this pathway is likely to operate *in vivo*.

In summary, these simulated data suggest that not only is $CheY_6$ a key regulator of flagellar motor rotation in *R. sphaeroides*, but it also acts as a "phosphate sink" ensuring rapid dephosphorylation of the other chemotaxis RRs (Figure 3A). This is very different from the *S. meliloti* sink where the sink CheY does not bind to the flagellar motor.

## The phosphatase activity of $CheA_3$ is required for $CheY_6$ to work as an efficient phosphate sink

In addition to containing the Hpt domain needed for phosphorylation of $CheY_6$, $CheA_3$ is also a phosphatase specific for $CheY_6$-P. This phosphatase activity has previously been shown to be essential for chemotaxis [48]. We used the model to determine the effect of phosphatase removal on RR-P levels and signal termination times, by setting the rate constants for the $CheA_3$ phosphatase reactions (15a) and (15b) in Table 2 to zero. The model predicted very high steady state concentrations of all of the RR-Ps (Table 5), with phosphorylation levels of the total chemotaxis RR pool rising from ~55% to ~97%. This was the result of increased levels of $CheY_6$-P (due to decreased dephosphorylation) leading to higher $CheA_2$-P and $CheA_3$-P concentrations and therefore higher levels of the other RR-Ps. The model also predicted that the signal termination times for all of the RR-Ps would be longer without the phosphatase (Table 4), as $CheY_6$ would be less effective as a phosphate sink for the other RR-Ps. The model therefore highlights the importance of the phosphatase activity in $CheA_3$, and demonstrates that although it is specific for $CheY_6$-P, the phosphatase activity indirectly affects the concentration of the other RR-Ps and their signal termination rates as outlined above (Figure 3A). Removal of the phosphatase activity is therefore predicted to cause a general increase in RR-P levels, which could account for the non-chemotactic phenotype of the strains lacking phosphatase activity [48].

## A phosphorelay pathway connects both chemotaxis clusters

We modeled the consequences of chemoeffector stimulation of either of the two chemotaxis clusters by either (i) turning off $CheA_2$ autophosphorylation (reaction (1) – parameter $k_1$ set to zero) to mimic attractant stimulation of the polar chemotaxis cluster or (ii) turning off the phosphorylation of $CheA_3$ by $CheA_4$ (reaction (2) – parameter $k_2$ set to zero) to mimic attractant stimulation of the cytoplasmic chemotaxis cluster (Figure 4). As expected, when $CheA_2$ autophosphorylation was turned off (case (i)) there was a reduction in the phosphorylation levels of each of the RRs (Figure 4) because $CheA_2$-P serves as a phosphodonor for all of the RRs. However, counter-intuitively, significant levels of all RR-Ps

**Table 4.** Comparison of RR-P autodephosphorylation rates with the RR-P dephosphorylation half-times predicted by the model.

| | | Dephosphorylation half-time predicted by simulation (s)[†] | | | | | | |
|---|---|---|---|---|---|---|---|---|
| | **Autodephosphorylation half-time (s)[*]** | **Wild type cells** | **Δ*cheY*$_3$** | **Δ*cheY*$_4$** | **Δ*cheY*$_6$** | **Δ*cheB*$_1$** | **Δ*cheB*$_2$** | **No phosphatase[‡]** |
| $CheY_3$-P | 36±3 | 4.9 | n/a | 4.7 | 296 | 3.7 | 5.2 | 8.4 |
| $CheY_4$-P | 38±3 | 7.3 | 7.3 | n/a | 543 | 5.1 | 8.1 | 15.1 |
| $CheY_6$-P | 4.1±0.3 | 1.3 | 1.3 | 1.4 | n/a | 1.3 | 1.3 | 8.2 |
| $CheB_1$-P | 4046±150 | 4.2 | 4.2 | 4.0 | 309 | n/a | 4.5 | 8.1 |
| $CheB_2$-P | 52±4 | 4.8 | 4.9 | 4.8 | 430 | 4.1 | n/a | 6.3 |

[*]These values were calculated from the experimentally determined *in vitro* autodephosphorylation rate constants [48].
[†]The model was allowed to reach a steady state where $CheA_2$ autophosphorylation (reaction 1) and the phosphorylation of $CheA_3$ by $CheA_4$ (reaction 2) were both active. Then reactions 1 and 2 were turned off. These half-times represent the time taken for levels of each of the RR-Ps to fall to half of their steady state values. Deletion of RRs was simulated by setting their total concentration in the model to zero, e.g. for Δ*cheY*$_3$, $Y_{3T}=0$ (Table 2).
[‡]Lack of $CheA_3$ phosphatase activity was simulated by setting $k_{15a}=k_{15b}=0$ (Table 2).
doi:10.1371/journal.pcbi.1000896.t004

remained, including $CheY_3$-P, $CheY_4$-P and $CheB_1$-P, which can only be generated by $CheA_2$-P.

Analysis of the modeling results from case (i) revealed that even though $CheA_2$ autophosphorylation had been turned off, significant levels of $CheA_2$-P were present and were being generated by the reversal of reaction (7) (Table 1) i.e. $CheB_2$-P was acting as a phosphodonor for $CheA_2$ (as demonstrated in Figure 2C). In this case, $CheY_6$ and $CheB_2$ were phosphorylated by $CheA_3$-P; $CheB_2$-P then served as a phosphodonor for $CheA_2$ i.e. $CheB_2$ transfers phosphoryl groups between $CheA_3$-P and $CheA_2$. The $CheA_2$-P generated in this way could then phosphorylate $CheY_3$, $CheY_4$ and $CheB_1$. This result suggests that $CheA_3$-P is linked to the RRs, $CheY_3$, $CheY_4$ and $CheB_1$, via a multistep phosphorelay i.e. $CheA_3$-P (His) to $CheB_2$ (Asp) to $CheA_2$ (His) to $CheY_3$/$CheY_4$/$CheB_1$ (Asp).

In case (ii), switching off the phosphorylation of $CheA_3$ by $CheA_4$ caused a reduction not only in the levels of $CheY_6$-P and $CheB_2$-P, but also in levels of $CheY_3$-P, $CheY_4$-P and $CheB_1$-P. Levels of $CheY_3$-P, $CheY_4$-P and $CheB_1$-P were affected because (a) they were dephosphorylated faster since the reduction in $CheY_6$-P levels was accompanied by an increase in the unphosphorylated $CheY_6$ levels which acts as a phosphate sink and (b) there was no input of phosphoryl groups at the cytoplasmic cluster for $CheB_2$ to transfer to these RRs via $CheA_2$. These results indicate that even when $CheA_2$ autophosphorylation is occurring, the bifunctional kinase/phosphatase in the cytoplasmic chemotaxis cluster makes a significant contribution to the phosphorylation levels of all of the RRs.

We performed a sensitivity analysis to look at the effect of varying each of the model parameters on levels of $CheY_4$-P when $CheA_2$

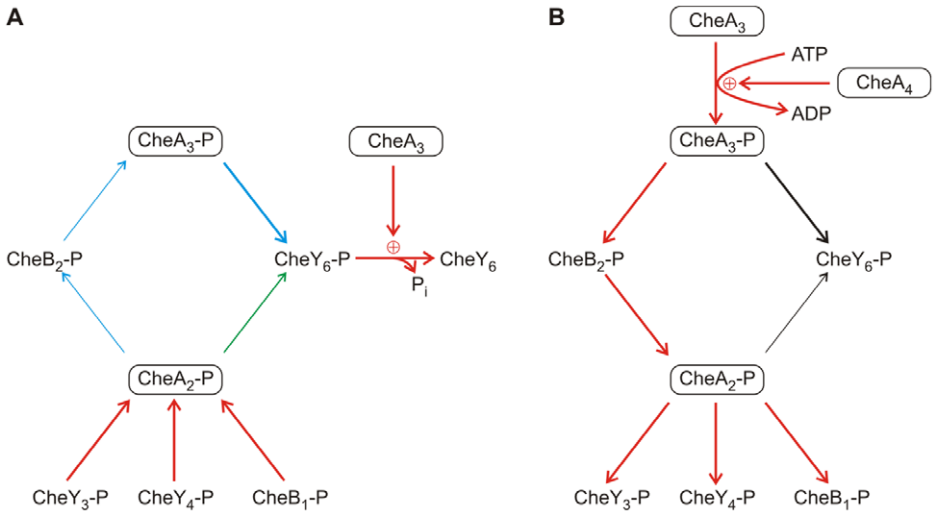


**Figure 3. Summary of the phosphate-sink and phosphorelay pathways.** (A) The phosphotransfer reactions that allow $CheY_6$ to work as a phosphate-sink for the other RR-Ps. $CheY_3$-P, $CheY_4$-P, $CheB_1$-P can act as phosphodonors for $CheA_2$. Phosphoryl groups can take either of two routes from $CheA_2$ to the $CheY_6$-phosphate-sink. $CheA_2$-P can directly phosphorylate $CheY_6$ (shown in green) or alternatively, can phosphorylate $CheB_2$, which can transfer the phosphoryl group to $CheA_3$ which then phosphorylates $CheY_6$ (shown in blue). $CheY_6$-P is rapidly dephosphorylated due to the specific phosphatase activity of the bifunctional enzyme $CheA_3$. For diagrammatic simplicity, reversible reactions are shown as operating in the direction that leads towards the sink. (B) Diagram summarizing the role of $CheB_2$ and $CheA_2$ in relaying phosphoryl groups from $CheA_3$-P to its non-cognate RRs, $CheY_3$, $CheY_4$ and $CheB_1$. The reactions necessary for this phosphorelay are highlighted in red. At the cytoplasmic chemotaxis cluster, phosphoryl groups are transferred from $CheA_3$-P to $CheY_6$ and $CheB_2$. $CheB_2$-P then diffuses to the polar chemotaxis cluster where it serves as a phosphodonor for $CheA_2$. $CheA_2$-P subsequently acts as a phosphodonor for $CheY_3$, $CheY_4$ and $CheB_1$. For diagrammatic simplicity, reactions which are reversible are shown as operating in the direction that leads towards the non-cognate RRs of $CheA_3$.
doi:10.1371/journal.pcbi.1000896.g003

**Table 5.** Comparison of steady state levels of RR-P with and without $CheA_3$ phosphatase activity.

| | Fraction phosphorylated (%) | |
|---|---|---|
| **Protein** | **Wild-type cells** | **No phosphatase**‡ |
| $CheY_3$ | 30 | 88 |
| $CheY_4$ | 75 | 98 |
| $CheY_6$ | 64 | 99 |
| $CheB_1$ | 33 | 91 |
| $CheB_2$ | 40 | 96 |
| Total RR pool | 55 | 97 |

‡Lack of $CheA_3$ phosphatase activity was simulated by setting $k_{15a} = k_{15b} = 0$ (Table 2).

doi:10.1371/journal.pcbi.1000896.t005

autophosphorylation is turned off; under these conditions $CheY_4$-P levels give a measure of the extent to which the phosphorelay is occurring (Table S2). The system was robust to changes in many of the parameters although as would be expected was sensitive to changes in parameters that directly affect either i) the rate of entry or exit of phosphoryl groups from the system e.g. rate of phosphorylation of $CheA_3$ by $CheA_4$, rate of $CheY_6$-P dephosphorylation (autodephosphorylation and phosphatase assisted), and the expression levels of $CheA_3$ and $CheY_6$ or ii) the functioning of the phosphorelay e.g. the expression levels of $CheA_2$ and $CheB_2$, rates of phosphotransfer between $CheA_3$ and $CheB_2$, between $CheB_2$ and $CheA_2$, and between $CheA_2$ and $CheY_4$. However, despite this sensitivity in almost all cases at least some phosphorylation of $CheY_4$ was predicted indicating that the phosphorelay remained operational. In the two remaining extreme cases, where $CheY_6$ expression levels were ten times higher than usual or where the rate of phosphorylation of $CheA_3$ by $CheA_4$ was ten-fold lower than the measured rate, levels of all RR-Ps, not just $CheY_4$-P, were extremely low. These results indicate that the phosphorelay operates over a broad range of parameter space, although the extent to which it operates is sensitive to large changes in some of the parameters.

## Discussion

The experimental work leading up to this study produced an outline architecture of the complex signaling network controlling *R. sphaeroides* chemotaxis [30]. However, the mechanism of integrating the signals produced by each of the signaling clusters to control the flagellar motor was unclear. Mathematical modeling has provided considerable insight into the probable functioning of simpler chemotaxis pathways [2,5,55], and a control engineering approach has recently been used in *R. sphaeroides* to discriminate between several possible mechanisms of CheY control of the flagellar motor [56]. In this study, a mathematical model of *R. sphaeroides* chemotaxis was formulated that integrates *in vivo* and *in vitro* biochemical data on the kinetic preferences of the signaling reactions with *in vivo* measurements of protein copy number. Analysis of the model revealed two

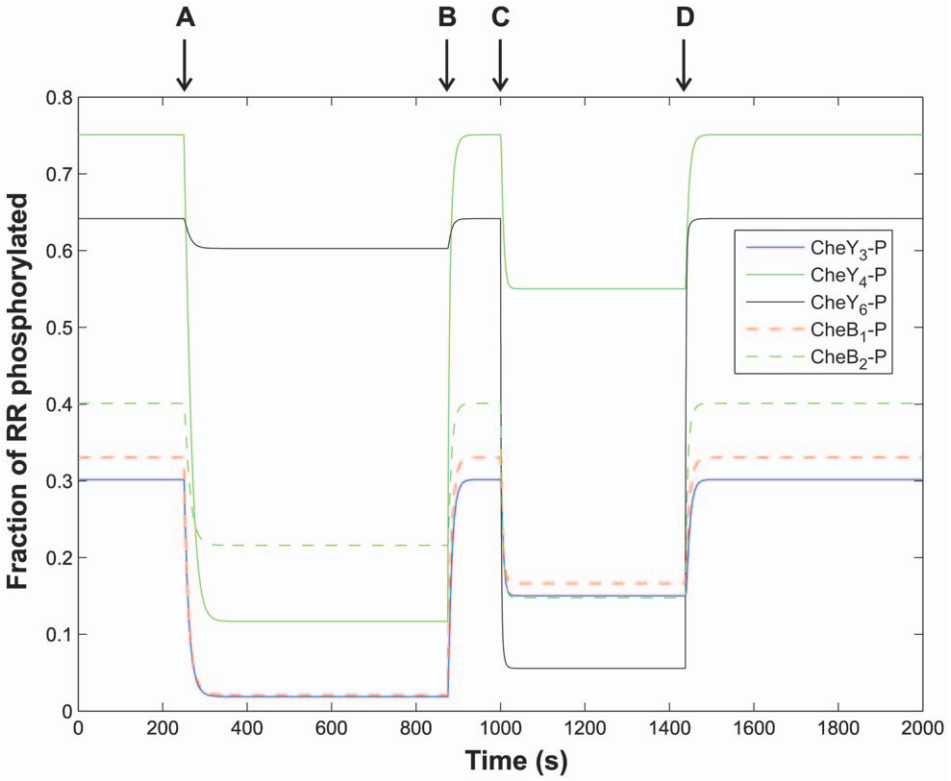


**Figure 4. The predicted variation in levels of RR-P throughout a simulated chemotaxis response.** Initially, $CheA_2$ autophosphorylation in the polar cluster and the phosphorylation of $CheA_3$ by $CheA_4$ in the cytoplasmic cluster are occurring. To mimic attractant stimulation of the polar cluster, $CheA_2$ autophosphorylation is turned off ($k_1 = 0$) at the point labelled (A). This causes a drop in RR-P levels and a new steady state is reached. (B) Subsequently, $CheA_2$ autophosphorylation is turned back on and the system returns to its original steady state. At point (C), the phosphorylation of $CheA_3$ by $CheA_4$ is turned off ($k_2 = 0$) to mimic attractant stimulation of the cytoplasmic cluster. As a result of this, RR-P levels fall and a new steady state is reached. (D) Finally, phosphorylation of $CheA_3$ by $CheA_4$ is turned back on and the system returns to its initial steady state.

doi:10.1371/journal.pcbi.1000896.g004

interesting features of the signaling network, both of which rely on reversed phosphotransfer from RR-Ps to CheA. Firstly, rapid signal termination for all chemotaxis RR-Ps may be achieved by $CheY_6$ acting as a phosphate sink in addition to being the primary motor control protein (Figure 3A). Secondly, a novel phosphorelay involving $CheB_2$ appears to link the cytoplasmic and polar chemotaxis clusters (Figure 3B). Together these two network features provide the bifunctional kinase/phosphatase, $CheA_3$, with the means to increase or decrease the concentration of all of the chemotaxis RR-Ps and therefore to regulate the output of the two chemosensory clusters.

## $CheY_6$ is a phosphate sink for all of the chemotaxis RR-Ps

Phosphate sinks provide an alternative mechanism for dephosphorylating RR-Ps [51,52], instead of simply hydrolyzing the phosphoryl group (as in autodephosphorylation or phosphatase-assisted-dephosphorylation), the phosphoryl group is transferred to a HPK, which subsequently transfers it to the "phosphate sink" RR. The phosphoryl group is then hydrolyzed from the "phosphate sink" by either autodephosphorylation or phosphatase-assisted-dephosphorylation. The model presented in this study predicted that signal termination occurs rapidly in *R. sphaeroides*, with all RR-Ps dephosphorylating with half-times of less than ~7 s (Table 4). This is consistent with the observed stimulus response time of 1 s for *R. sphaeroides* [50], since with a decay half-time of ~7 s, CheY-P levels could fall by ~10% during 1s, which, assuming that the *R. sphaeroides* motor is as ultrasensitive to changes in CheY-P levels as the *E. coli* motor [57], would be sufficient to give a significant change in motor rotation bias.

Prior to this study, it was known that $CheY_6$-P with the aid of its specific phosphatase, the bifunctional protein $CheA_3$, could dephosphorylate rapidly [48], however, the other RR-Ps were known to autodephosphorylate with half-times in excess of 36 s, with $CheB_1$-P taking over 4000 s. By removing each of the RRs in turn from the model, we found that $CheY_6$ was acting as a "phosphate sink" for the other RR-Ps, since cells lacking $CheY_6$ showed much slower dephosphorylation rates for the remaining RR-Ps (Table 4 and Figure 3A). Furthermore, we showed that removal of the phosphatase activity of $CheA_3$ from the model increased the dephosphorylation half-times of all of the RR-Ps, indicating that the phosphatase activity is required for efficient operation of the $CheY_6$ phosphate sink and rapid signal termination. This phosphate sink role for $CheY_6$ is additional to its primary role as a direct regulator of flagellar rotation [39].

$CheY_6$ differs in several ways from the prototypical phosphate sink, CheY1 from *S. meliloti* [51]. $CheY_6$ directly controls flagellar motor rotation by binding FliM [39,49], and has a dedicated phosphatase, in contrast, *S. meliloti* CheY1 does not bind FliM and appears to function only as a "phosphate sink". Another fundamental difference is the rate of dephosphorylation; $CheY_6$-P dephosphorylates much faster than the autodephosphorylation rates of the RRs for which it acts as a sink whereas *S. meliloti* CheY1-P does not autodephosphorylate any faster than the motor binding RR, CheY2-P, for which it is a sink. The *S. meliloti* sink does not need to dephosphorylate quickly because it does not directly affect flagellar rotation and so phosphoryl groups can be stored on it until autodephosphorylation occurs, in contrast, *R. sphaeroides* $CheY_6$ is a key regulator of flagellar rotation and therefore requires rapid signal termination.

## A $CheB_2$ mediated phosphorelay connects the polar and cytoplasmic signaling clusters

As part of our interrogation of the model, we simulated attractant stimulation of the polar chemotaxis cluster by turning off autophosphorylation of $CheA_2$, while allowing phosphorylation of $CheA_3$ by $CheA_4$ to occur (Figure 4). Interestingly under these conditions, even though $CheA_3$-P cannot directly phosphorylate $CheY_3$, $CheY_4$, and $CheB_1$, the model predicted non-zero concentrations of these RR-Ps. This is the result of the action of a phosphorelay where phosphoryl groups from $CheA_3$-P (His) are transferred to $CheB_2$ (Asp) then to $CheA_2$ (His) and subsequently to either $CheY_3$, $CheY_4$ or $CheB_1$ (Asp) (Figure 3B). Direct testing of the *in vivo* importance of this phosphorelay is confounded by the dual role of $CheB_2$, firstly as a chemoreceptor methylesterase and secondly as a potential intermediate in the phosphorelay. The methylesterase activity of $CheB_2$ is required for normal chemotaxis and it is not possible to block the phosphorylation of $CheB_2$ by mutagenesis without impairing the control of this methylesterase activity. It is therefore not known the extent to which this $CheB_2$ mediated phosphorelay operates *in vivo*; however, the model does incorporate both *in vitro* kinetic preference data and *in vivo* protein expression levels, and this suggests that the phosphorelay may operate *in vivo*, allowing the cytoplasmic cluster to make a significant contribution to phosphorylation levels of the non-cognate RRs; $CheY_3$, $CheY_4$ and $CheB_1$.

The model in this study does not include adaptation as this is a poorly understood process in *R. sphaeroides*, with little experimental data. However, it is possible that the adaptation pathway could act to reduce the elevated RR-P levels caused by a constant influx of phosphoryl groups to the polar cluster from the cytoplasmic cluster by modifying the polar receptors in such a way as to reduce the autophosphorylation rate of the polar kinase, $CheA_2$ i.e. the cell could adapt to constant signals from the cytoplasmic cluster. Although when cells are performing chemotaxis and swimming through gradients of chemoeffector, signals from the cytoplasmic cluster will vary over time and will make a significant contribution to RR-P levels. The relative contribution of this phosphorelay to levels of $CheY_3$-P, $CheY_4$-P and $CheB_1$-P will be modulated by signals coming through the transmembrane chemoreceptors that directly control the rate of $CheA_2$ autophosphorylation and would be greatest when the autophosphorylation rate of $CheA_2$ is low and the rate of phosphorylation of $CheA_3$ by $CheA_4$ is high. These conditions could arise when cells are swimming up a gradient of a specific attractant which is sensed by the transmembrane chemoreceptors, while the metabolic state of the cell is worsening due to, for example, decreasing concentrations of an essential nutrient (for which there may not be a transmembrane chemoreceptor). Under such conditions, the increased rate of phosphorylation of $CheA_3$ by $CheA_4$, coupled with the $CheB_2$/$CheA_2$ mediated phosphorelay, could raise levels $CheY_3$-P, $CheY_4$-P and $CheY_6$-P, allowing cells to override their favourable response to the extracellular attractant and swim away from these unfavourable environments.

Numerous examples of other two-component systems employing phosphorelays have been described [58–61]; however, to the best of our knowledge this is the first example of a phosphorelay involving two distinct HPKs localized to different regions of the cell, and also, the first phosphorelay to be found in a chemotaxis signaling pathway. Given that over 50% of bacteria with any *che* genes have more than two *cheA*s [31,32,48], it seems likely that phosphorelays allowing communication between different CheA homologues could be involved in chemotactic signaling in a wide range of bacterial species.

## Signal integration by the cytoplasmic cluster

The polar cluster senses extracellular signals while the cytoplasmic cluster is believed to sense the metabolic state of the cell [30]. The concentration of each RR-P depends not only on polar kinase activity but also on the balance of kinase and phosphatase activity in

the cytoplasmic cluster. The kinase activity of the cytoplasmic cluster resides in $CheA_4$ and the phosphatase activity resides in $CheA_3$; both proteins have P5 (regulatory) domains and it is therefore likely that both activities will be regulated by environmental stimuli [48,62]. A stimulus that increases phosphatase activity would have the effect of reducing levels of all RR-Ps, since the action of the phosphatase would directly accelerate $CheY_6$-P dephosphorylation leaving more unphosphorylated $CheY_6$ to function as a phosphate sink for the other RR-Ps. Such a mechanism could allow the cytoplasmic cluster to tune or modulate signals coming from the polar cluster since increased phosphatase activity would lead to a general decrease in chemotaxis RR-P levels. In contrast, a stimulus that increased kinase activity at the cytoplasmic cluster would increase levels of all RR-Ps because $CheA_3$-P would phosphorylate $CheY_6$ and $CheB_2$ directly; $CheB_2$ would then shuttle the phosphoryl groups to $CheA_2$ and from there onto the other RRs while phosphorylation of $CheY_6$ would reduce its capacity as a phosphate sink resulting in a general increase in RR-P levels. Therefore the overall sensory output of the pathway depends critically on the relative activity of $CheA_3$ and $CheA_4$, and potentially provides a mechanism for signals about the metabolic state of the cell to modulate signals regarding the extracellular environment.

## Materials and Methods

### Mathematical model

Full details on the mathematical model are included in Text S1. Briefly, the law of mass action was applied to the reactions detailed in Table 1 to produce a system of non-linear ordinary differential equations (ODEs), which were solved using Matlab (MathWorks). The model was parameterized with data from the literature [39,43,45,48,63–65] and our own experiments as detailed in Tables 2&3. A parameter fit of the phosphotransfer rates between each kinase and RR (time course data) with that of a mathematical model describing the *in vitro* reactions was performed. A number of local, global and genetic algorithm optimisation procedures were employed (simulated annealing, Hooke and Jeeves, least squares, Levenberg-Marquardt, Nelder-Mead, steepest descent and the genetic algorithm) to obtain a robust set of parameters (Table 3).

### Plasmids and strains

The plasmids and strains used are shown in Table S3. *E. coli* strains were grown in LB medium at 37°C. Where required, antibiotics were used at concentrations of 100 μg $ml^{-1}$ for ampicillin and 25 μg $ml^{-1}$ for kanamycin.

### Protein purification

His-tagged and GST-tagged *R. sphaeroides* CheA, CheY and CheB proteins were purified as described previously [66]. Protein purity and concentration was measured as described [45]. Purified proteins were stored at −20°C.

### Preparation of $CheA_3P1$-$^{32}P$

$CheA_3P1$ was phosphorylated using [$\gamma$-$^{32}P$] ATP and $CheA_4$, and purified as described previously [48]. The final preparation of $CheA_3P1$-$^{32}P$ was free of ATP and $CheA_4$.

### Detection of phosphotransfer from the response regulators to $CheA_2$

Assays were performed at 20°C in TGMNKD buffer (50 mM Tris HCl, 10% (v/v) glycerol, 5 mM $MgCl_2$, 150 mM NaCl, 50 mM KCl, 1 mM DTT, pH 8.0). $CheA_3P1$-$^{32}P$ was used to phosphorylate the RRs, $CheY_6$ and $CheB_2$, in these assays because it is a good phosphodonor for these proteins and even after prolonged incubation (>1 hour) $CheA_3P1$-$^{32}P$ does not act as a direct phosphodonor for $CheA_2$ (Figure 3A); therefore any $CheA_2$-P generated in these assays is due to phosphotransfer from RR-P to $CheA_2$ rather than direct phosphotransfer from $CheA_3P1$-P to $CheA_2$. 30 μM $CheA_3P1$-$^{32}P$ was mixed with 5 μM $CheA_2$ prior to the addition of 10 μM RR. Following the addition of RR, reaction aliquots of 10 μl were taken at the indicated timepoints and quenched immediately in 5 μl of 3 X SDS-PAGE loading dye (7.5% (w/v) SDS, 90 mM EDTA, 37.5 mM Tris HCl, 37.5% glycerol, 3% (v/v) β-mercaptoethanol, pH 6.8). Quenched samples were analyzed using SDS-PAGE and phosphorimaging as described previously.

### Protein expression levels

Protein expression levels were measured in wild-type *R. sphaeroides* cells grown under microaerobic growth conditions using quantitative immunoblotting as described previously [65,67–69].

## Supporting Information

**Table S1** The effect of parameter variation on the simulation half-life of $CheB_1$-P.
Found at: doi:10.1371/journal.pcbi.1000896.s001 (0.09 MB PDF)

**Table S2** The effect of parameter variation on the predicted levels of $CheY_4$-P when $CheA_2$ autophosphorylation is turned off ($k_1 = 0$).
Found at: doi:10.1371/journal.pcbi.1000896.s002 (0.09 MB PDF)

**Table S3** Plasmids and bacterial strains used in this study.
Found at: doi:10.1371/journal.pcbi.1000896.s003 (0.01 MB PDF)

**Text S1** Mathematical modeling.
Found at: doi:10.1371/journal.pcbi.1000896.s004 (0.02 MB PDF)

## Author Contributions

Conceived and designed the experiments: MJT SLP PKM JPA. Performed the experiments: SLP. Analyzed the data: MJT SLP. Contributed reagents/materials/analysis tools: MJT SLP. Wrote the paper: MJT SLP PKM JPA.

## References


1. Stock AM, Robinson VL, Goudreau PN (2000) Two-component signal transduction. Annu Rev Biochem 69: 183–215.
2. Bray D, Levin MD, Morton FC (1998) Receptor clustering as a cellular mechanism to control sensitivity. Nature 393: 85–88.
3. Tindall MJ, Maini PK, Porter SL, Armitage JP (2008) Overview of mathematical approaches used to model bacterial chemotaxis II: bacterial populations. Bull Math Biol 70: 1570–1607.
4. Tindall MJ, Porter SL, Maini PK, Gaglia G, Armitage JP (2008) Overview of mathematical approaches used to model bacterial chemotaxis I: the single cell. Bull Math Biol 70: 1525–1569.
5. Hansen CH, Endres RG, Wingreen NS (2008) Chemotaxis in *Escherichia coli*: a molecular model for robust precise adaptation. PLoS Comput Biol 4: e1.
6. Tu Y, Shimizu TS, Berg HC (2008) Modeling the chemotactic response of *Escherichia coli* to time-varying stimuli. Proc Natl Acad Sci USA 105: 14855–14860.
7. Endres RG, Oleksiuk O, Hansen CH, Meir Y, Sourjik V, et al. (2008) Variable sizes of *Escherichia coli* chemoreceptor signaling teams. Mol Syst Biol 4: 211.
8. Goldman JP, Levin MD, Bray D (2009) Signal amplification in a lattice of coupled protein kinases. Mol BioSyst 5: 1853–1859.
9. Rao CV, Kirby JR, Arkin AP (2004) Design and diversity in bacterial chemotaxis: a comparative study in *Escherichia coli* and *Bacillus subtilis*. PLoS Biol 2: e49.
10. Alon U, Surette MG, Barkai N, Leibler S (1999) Robustness in bacterial chemotaxis. Nature 397: 168–171.

11. Hazelbauer GL, Falke JJ, Parkinson JS (2008) Bacterial chemoreceptors: high-performance signaling in networked arrays. Trends Biochem Sci 33: 9–19.
12. Wadhams GH, Armitage JP (2004) Making sense of it all: Bacterial chemotaxis. Nat Rev Mol Cell Bio 5: 1024–1037.
13. Szurmant H, Ordal GW (2004) Diversity in chemotaxis mechanisms among the Bacteria and Archaea. Microbiol Mol Biol Rev 68: 301–319.
14. Maddock JR, Shapiro L (1993) Polar location of the chemoreceptor complex in the *Escherichia coli* cell. Science 259: 1717–1723.
15. Greenfield D, McEvoy AL, Shroff H, Crooks GE, Wingreen NS, et al. (2009) Self-organization of the *Escherichia coli* chemotaxis network imaged with super-resolution light microscopy. PLoS Biol 7: e1000137.
16. Briegel A, Ortega DR, Tocheva EI, Wuichet K, Li Z, et al. (2009) Universal architecture of bacterial chemoreceptor arrays. Proc Natl Acad Sci USA 106: 17181–17186.
17. Borkovich KA, Kaplan N, Hess JF, Simon MI (1989) Transmembrane signal transduction in bacterial chemotaxis involves ligand-dependent activation of phosphate group transfer. Proc Natl Acad Sci USA 86: 1208–1212.
18. Ninfa EG, Stock A, Mowbray S, Stock J (1991) Reconstruction of the bacterial chemotaxis signal transduction system from purified components. J Biol Chem 266: 9764–9770.
19. Boldog T, Grimme S, Li M, Sligar SG, Hazelbauer GL (2006) Nanodiscs separate chemoreceptor oligomeric states and reveal their signaling properties. Proc Natl Acad Sci USA 103: 11509–11514.
20. Hess JF, Bourret RB, Simon MI (1988) Histidine phosphorylation and phosphoryl group transfer in bacterial chemotaxis. Nature 336: 139–143.
21. Sanders DA, Gillece-Castro BL, Stock AM, Burlingame AL, Koshland DE Jr (1989) Identification of the site of phosphorylation of the chemotaxis response regulator protein, CheY. J Biol Chem 264: 21770–21778.
22. Bourret RB, Hess JF, Simon MI (1990) Conserved aspartate residues and phosphorylation in signal transduction by the chemotaxis protein CheY. Proc Natl Acad Sci USA 87: 41–45.
23. Welch M, Oosawa K, Aizawa S-I, Eisenbach M (1993) Phosphorylation-dependent binding of a signal molecule to the flagellar switch of bacteria. Proc Natl Acad Sci USA 90: 8787–8791.
24. Dyer CM, Vartanian AS, Zhou H, Dahlquist FW (2009) A Molecular Mechanism of Bacterial Flagellar Motor Switching. J Mol Biol 388: 71–84.
25. Lupas A, Stock J (1989) Phosphorylation of an N-terminal regulatory domain activates the CheB methylesterase in bacterial chemotaxis. J Biol Chem 264: 17337–17342.
26. Sourjik V, Berg HC (2002) Receptor sensitivity in bacterial chemotaxis. Proc Natl Acad Sci USA 99: 123–127.
27. Thomas SA, Brewster JA, Bourret RB (2008) Two variable active site residues modulate response regulator phosphoryl group stability. Mol Microbiol 69: 453–465.
28. Hess JF, Oosawa K, Kaplan N, Simon MI (1988) Phosphorylation of three proteins in the signalling pathway of bacterial chemotaxis. Cell 53: 79–87.
29. Silversmith RE, Levin MD, Schilling E, Bourret RB (2008) Kinetic characterization of catalysis by the chemotaxis phosphatase CheZ: modulation of activity by the phosphorylated CheY substrate. J Biol Chem 283: 756–765.
30. Porter SL, Wadhams GH, Armitage JP (2008) *Rhodobacter sphaeroides*: Complexity in chemotactic signalling. Trends Microbiol 16: 251–260.
31. Hamer R, Chen P-Y, Armitage JP, Reinert G, Deane CM (2010) Deciphering chemotaxis pathways using cross species comparisons. BMC Syst Biol 4: 3.
32. Wuichet K, Zhulin IB (2010) Origins and diversification of a complex signal transduction system in prokaryotes. Sci Signal 3: ra50.
33. Armitage JP, Macnab RM (1987) Unidirectional intermittent rotation of the flagellum of *Rhodobacter sphaeroides*. J Bacteriol 169: 514–518.
34. Porter SL, Warren AV, Martin AC, Armitage JP (2002) The third chemotaxis locus of *Rhodobacter sphaeroides* is essential for chemotaxis. Mol Microbiol 46: 1081–1094.
35. Martin AC, Wadhams GH, Armitage JP (2001) The roles of the multiple CheW and CheA homologues in chemotaxis and in chemoreceptor localization in *Rhodobacter sphaeroides*. Mol Microbiol 40: 1261–1272.
36. Pilizota T, Brown MT, Leake MC, Branch RW, Berry RM, et al. (2009) A molecular brake, not a clutch, stops the *Rhodobacter sphaeroides* flagellar motor. Proc Natl Acad Sci USA 106: 11582–11587.
37. Poggio S, breu-Goodger C, Fabela S, Osorio A, Dreyfus G, et al. (2007) A complete set of flagellar genes acquired by horizontal transfer coexists with the endogenous flagellar system in *Rhodobacter sphaeroides*. J Bacteriol 189: 3208–3216.
38. del Campo AM, Ballado T, de la Mora J, Poggio S, Camarena L, et al. (2007) Chemotactic control of the two flagellar systems of *Rhodobacter sphaeroides* is mediated by different sets of CheY and FliM proteins. J Bacteriol 189: 8397–8401.
39. Porter SL, Wadhams GH, Martin AC, Byles ED, Lancaster DE, et al. (2006) The CheYs of *Rhodobacter sphaeroides*. J Biol Chem 281: 32694–32704.
40. Martin AC, Wadhams GH, Shah DSH, Porter SL, Mantotta JC, et al. (2001) CheR- and CheB-dependent chemosensory adaptation system of *Rhodobacter sphaeroides*. J Bacteriol 183: 7135–7144.
41. Shah DSH, Porter SL, Martin AC, Hamblin PA, Armitage JP (2000) Fine tuning bacterial chemotaxis: analysis of *Rhodobacter sphaeroides* behaviour under aerobic and anaerobic conditions by mutation of the major chemotaxis operons and *cheY* genes. EMBO J 19: 4601–4613.
42. Shah DS, Porter SL, Harris DC, Wadhams GH, Hamblin PA, et al. (2000) Identification of a fourth *cheY* gene in *Rhodobacter sphaeroides* and interspecies interaction within the bacterial chemotaxis signal transduction pathway. Mol Microbiol 35: 101–112.
43. Porter SL, Armitage JP (2004) Chemotaxis in *Rhodobacter sphaeroides* requires an atypical histidine protein kinase. J Biol Chem 279: 54573–54580.
44. Wadhams GH, Warren AV, Martin AC, Armitage JP (2003) Targeting of two signal transduction pathways to different regions of the bacterial cell. Mol Microbiol 50: 763–770.
45. Porter SL, Armitage JP (2002) Phosphotransfer in *Rhodobacter sphaeroides* chemotaxis. J Mol Biol 324: 35–45.
46. Wadhams GH, Martin AC, Porter SL, Maddock JR, Mantotta JC, et al. (2002) TlpC, a novel chemotaxis protein in *Rhodobacter sphaeroides*, localizes to a discrete region in the cytoplasm. Mol Microbiol 46: 1211–1221.
47. Bell CH, Porter SL, Strawson A, Stuart DI, Armitage JP (2010) Using structural information to change the phosphotransfer specificity of a two-component chemotaxis signalling complex. PLoS Biol 8: e1000306.
48. Porter SL, Roberts MAJ, Manning CS, Armitage JP (2008) A bifunctional kinase-phosphatase in bacterial chemotaxis. Proc Natl Acad Sci USA 105: 18531–18536.
49. Ferre A, de la Mora J, Ballado T, Camarena L, Dreyfus G (2004) Biochemical study of multiple CheY response regulators of the chemotactic pathway of *Rhodobacter sphaeroides*. J Bacteriol 186: 5172–5177.
50. Berry RM, Armitage JP (2000) Response kinetics of tethered *Rhodobacter sphaeroides* to changes in light intensity. Biophys J 78: 1207–1215.
51. Sourjik V, Schmitt R (1998) Phosphotransfer between CheA, CheY1, and CheY2 in the chemotaxis signal transduction chain of *Rhizobium meliloti*. Biochemistry 37: 2327–2335.
52. Jimenez-Pearson MA, Delany I, Scarlato V, Beier D (2005) Phosphate flow in the chemotactic response system of *Helicobacter pylori*. Microbiology 151: 3299–3311.
53. Rasmussen AA, Porter SL, Armitage JP, Sogaard-Andersen L (2005) Coupling of multicellular morphogenesis and cellular differentiation by an unusual hybrid histidine protein kinase in *Myxococcus xanthus*. Mol Microbiol 56: 1358–1372.
54. Rasmussen AA, Wegener-Feldbrugge S, Porter SL, Armitage JP, Sogaard-Andersen L (2006) Four signalling domains in the hybrid histidine protein kinase RodK of *Myxococcus xanthus* are required for activity. Mol Microbiol 60: 525–534.
55. Tindall MJ, Porter SL, Wadhams GH, Maini PK, Armitage JP (2009) Spatiotemporal modelling of CheY complexes in *Escherichia coli* chemotaxis. Prog Biophys Mol Biol 100: 40–46.
56. Roberts M, August E, Hamadeh A, Maini P, McSharry P, et al. (2009) A model invalidation-based approach for elucidating biological signalling pathways, applied to the chemotaxis pathway in *R. sphaeroides*. BMC Syst Biol 3: 105.
57. Cluzel P, Surette M, Leibler S (2000) An ultrasensitive bacterial motor revealed by monitoring signaling proteins in single cells. Science 287: 1652–1655.
58. Mitrophanov AY, Groisman EA (2008) Signal integration in bacterial two-component regulatory systems. Genes Dev 22: 2601–2611.
59. Perego M, Hanstein C, Welsh KM, Djavakhishvili T, Glaser P, et al. (1994) Multiple protein-aspartate phosphatases provide a mechanism for the integration of diverse signals in the control of development in *B. subtilis*. Cell 79: 1047–1055.
60. Ogino T, Matsubara M, Kato N, Nakamura Y, Mizuno T (1998) An *Escherichia coli* protein that exhibits phosphohistidine phosphatase activity towards the HPt domain of the ArcB sensor involved in the multistep His-Asp phosphorelay. Mol Microbiol 27: 573–585.
61. Appleby JL, Parkinson JS, Bourret RB (1996) Signal transduction via the multi-step phosphorelay: not necessarily a road less traveled. Cell 86: 845–848.
62. Scott KA, Porter SL, Bagg EAL, Hamer R, Hill JL, et al. (2010) Specificity of localization and phosphotransfer in the CheA proteins of *Rhodobacter sphaeroides*. Mol Microbiol 76: 318–330.
63. Slovak PM, Porter SL, Armitage JP (2006) Differential localization of Mre proteins with PBP2 in *Rhodobacter sphaeroides*. J Bacteriol 188: 1691–1700.
64. Slovak PM, Wadhams GH, Armitage JP (2005) Localization of MreB in *Rhodobacter sphaeroides* under conditions causing changes in cell shape and membrane structure. J Bacteriol 187: 54–64.
65. Ind AC, Porter SL, Brown MT, Byles ED, de Beyer JA, et al. (2009) An inducible expression plasmid for *Rhodobacter sphaeroides* and *Paracoccus denitrificans*. Appl Environ Microbiol 75: 6613–6615.
66. Porter SL, Wadhams GH, Armitage JP (2007) *In vivo* and *in vitro* analysis of the *Rhodobacter sphaeroides* chemotaxis signaling complexes. Method Enzymol 423: 392–413.
67. Ben-Anat Porat Y, Zan-Bar I, Ravid A (1995) Quantitative dot-blot assay for low titer anti-lipopolysaccharide antibodies in human plasma. J Immunol Methods 180: 213–218.
68. Brown MT (2009) Control of the unidirectional motor in *Rhodobacter sphaeroides*. D. Phil. Thesis. University of Oxford.
69. Gould, Marcus (2006) Chemotaxis gene expression in *Rhodobacter sphaeroides* WS8N. D. Phil. Thesis. University of Oxford.